However, all three precursors, 2-4, provided only very small amounts of a radical cation with m/z 98, while this fragment represents the second most frequent ion in the case of 1. Apparently, 2 decomposed under the applied experimental conditions and 3 predominantly formed CH-containing fragments with m/z 98 and 100. Only 4 produced $H_2S_2O_2^{\bullet+}$ in an abundance sufficient for an NRMS experiment. But, unfortunately, both the CA and NR spectra are beyond a detailed interpretation due to interfering decomposition products from the ion source.

Conclusion

Electron-impact-induced dissociation of diisopropoxy disulfide in the vapor phase yields propene and the chainlike radical cation $HOSSOH^{\bullet+}$, which was neutralized in a NRMS experiment to give the free acid HOSSOH. In the highly diluted gas phase, this molecule is stable against isomerization during the time of its observation (10^{-5} s), indicating that isomer I is separated from isomers of comparable energy, like HOS(O)SH (II), by a sufficiently high energy barrier. Isomerization of I to give II probably has to proceed via III (migration of an OH group from one sulfur to the other) followed by a proton shift from oxygen to the terminal sulfur atom which becomes two-valent (eq 3). This two-step

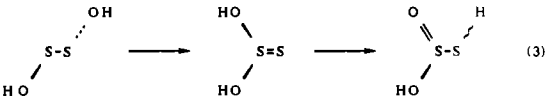

mechanism may explain that under the experimental conditions only I was observed when diisopropoxy disulfide was used as a precursor. On the other hand, dissociation of I into S_2O and H_2O may be more favorable than the isomerization due to a possibly lower energy barrier, thus explaining that II was not observed.

Attempts to obtain other isomers (II-IV) from corresponding precursors have failed so far. This does not exclude II from being generated in a totally different experiment. For instance, reaction 1 probably leads primarily to the adduct $H_2S{\cdot}SO_2$, containing a weak SS bond[19] which may stabilize itself by a proton shift to oxygen, resulting in II. Work to identify the initial products of reaction 1 is in progress.

Acknowledgment. Useful comments by one of the reviewers and financial support by the Deutsche Forschungsgemeinschaft, the Fonds der Chemischen Industrie, and the Graduiertenkolleg Chemie are gratefully appreciated.

(18) Compound 2 has been prepared from thionyl chloride, 2-propanol, and 2-mercaptopropane in the presence of triethylamine. It could not be obtained in pure form due to decomposition. 3 was kindly provided by D. N. Harpp. See also: Harpp, D. N.; Steliou, K.; Cheer, C. J. *J. Chem. Soc., Chem. Commun.* **1980**, 825. 4 has been prepared by the reaction of diisopropyl disulfide with sulfuryl chloride in the presence of acetic acid according to: Buckmann, J. D.; Bellas, M.; Kim, H. K.; Field, L.; *J. Org. Chem.* **1967**, *32*, 1626.

(19) See also the structure of the van der Waals molecule $H_2S{\cdot}SO_2$ in: Kukolich, S. G.; Pauley, D. J. *J. Chem. Phys.* **1990**, *93*, 871.

Contribution from the Department of Chemistry, Stanford University, Stanford, California 94305

Single-Crystal Polarized Absorption Spectroscopic Study of the Electronic Structure of μ-1,2-Peroxo Binuclear Cobalt Complexes

Felix Tuczek and Edward I. Solomon*

Received August 19, 1991

Single-crystal polarized absorption spectra of five trans planar μ-peroxo cobalt systems are presented and interpreted. Ligand field (LF) transitions are assigned at energies typical for Co(III) systems. Charge-transfer (CT) transitions from the peroxide π^*_v orbital vertical with respect to the Co-O-O-Co plane to the cobalt dσ orbitals are found to be at lower energy than the LF transitions. This indicates that the highest occupied molecular orbital (HOMO) of planar monobridged cobalt peroxo complexes has peroxide π^*_v character. Due to the limited overlap between the orbitals involved, the intensity of these CT transitions is low ($\epsilon \approx 100$ M^{-1} cm^{-1}). The overlap between the peroxide π^*_σ orbital within the Co-O-O-Co plane and the cobalt d_{z^2} orbital is large. The intense band ($\epsilon = 14\,000$ M^{-1} cm^{-1}) at 300 nm is assigned to the $\pi^*_\sigma \rightarrow d_{z^2}$ CT transition, which is supported by the *A*-term Raman enhancement behavior observed for the intra-peroxide stretch. These results are related to the spectra of cis μ-1,2-peroxo cobalt the trans μ-1,2-superoxo cobalt complexes, and the photochemical implications of the different bonding schemes are discussed. A comparison of the spectra of the trans μ-peroxo cobalt and the trans μ-peroxo binuclear copper systems reveals characteristic differences with respect to dimer splitting in CT excited states.

Introduction

The reversible binding and activation of dioxygen by transition metal complexes has been of continued interest in biochemistry and in heterogeneous and homogeneous catalysis. Cobalt peroxo and superoxo complexes comprise a large number of structurally characterized monomers as well as cis and trans μ-1,2- and μ-1,1-hydroperoxo-bridged dimers. Thermodynamic, kinetic, and mechanistic aspects of interconversions between these species are well understood and have been reviewed.[1]

A comparison of the different binding modes of peroxide has gained considerable importance in connection with the question of which structural modes are involved in the binding and activation of oxygen in copper-containing enzymes. Hemocyanin and tyrosinase bind dioxygen as a bridge between two copper centers,[2a-c] and laccase reduces O_2 to H_2O via a peroxide-bridged intermediate at a trinuclear copper site.[2d] An understanding of the spectral features associated with different peroxide binding modes, particularly the peroxide to metal charge-transfer spectra, is of crucial importance for further mechanistic insight into binding and activation of oxygen in biomolecules. The variety of structurally characterized cobalt peroxo dimers allows a systematic comparison of these features. Spectroscopic studies along these lines are also of theoretical interest with respect to electronic interactions in dimers. Whereas attention has traditionally been focused on interactions in the electronic ground state, little has been done to investigate excited-state dimer interactions. In copper dimers, a detailed picture of dimer interactions in excited ligand

* To whom correspondence should be directed.

(1) (a) Niederhoffer, E. C.; Timmons, J. H.; Martell, A. E. *Chem. Rev.* **1984**, *84*, 137. (b) Jones, R. D.; Summerville, D. A.; Basolo, F. *Chem. Rev.* **1979**, *79*, 13.

(2) (a) Solomon, E. I.; Penfield, K. W.; Wilcox, D. E. *Struct. Bonding (Berlin)* **1983**, *53*, 1. (b) Solomon, E. I. *Pure Appl. Chem.* **1983**, *55*, 1069. (c) Solomon, E. I. In *Copper Proteins*; Spiro, T. G., Ed.; Wiley: New York, 1981; p 41. (d) Cole, J. L.; Clark, P. A.; Solomon, E. I. *J. Am. Chem. Soc.* **1990**, *112*, 9534.

0020-1669/92/1331-0944$03.00/0

field (LF) states has been obtained.[3] However, while significant spectral consequences of dimer interactions in charge-transfer transitions have been documented,[4] a comparable level of understanding has not yet been achieved.

A number of spectroscopic investigations have been carried out on cis and trans μ-1,2-peroxo cobalt complexes,[5-8] and reviews of their electronic structure have appeared.[9,10] Assignments have been based mainly on solution spectra. So far, no detailed single-crystal absorption study of these systems exists.[11] Correspondingly, a complete picture of the LF and CT spectra has not been achieved. In the present paper, solution and single-crystal optical as well as Raman spectroscopic measurements of structurally characterized trans planar μ-1,2-peroxo cobalt complexes will be presented and interpreted. In order to keep structural and electronic variations limited, only simple decaammine and analogous polydentate amine complexes are investigated. The results are compared with parallel data on a trans μ-1,2-peroxo copper dimer.[4a] CT excited-state splittings are expected to differ, since the copper(II) dimer is an open-shell system whereas the (low spin) cobalt(III) dimers are closed-shell systems. In addition, the monobridged peroxo cobalt dimers are compared to the dibridged cis μ-1,2-peroxo cobalt dimers and a trans μ-1,2-superoxo dimer.[12] The photochemical implications of the results will also be discussed.

Experimental Section

a. Preparation of Compounds. All procedures described below were adapted from the literature and modified to give crystals large enough for single-crystal optical absorption measurements (i.e. with faces larger than 1 mm × 1 mm). For easier reference, short notations are introduced for the five systems studied spectroscopically.

I. $[(NH_3)_5CoO_2Co(NH_3)_5]^{4+}$. Three different salts were prepared. The nitrate $[(NH_3)_5CoO_2Co(NH_3)_5](NO_3)_4 \cdot 2H_2O$[13] is not suitable for optical measurements, since the crystals lose water rapidly. Starting from this compound, a considerably more stable mixed salt $[(NH_3)_5CoO_2Co(NH_3)_5](NO_3)_2(SCN)_2 \cdot H_2O$ (notation: $[NH_3]NO_3SCN$) was obtained by adding thiocyanate to the solution of $Co(NO_3)_2$ in 7 M NH_3. This preparation was also carried out with $^{18}O_2$ in a closed apparatus. Single crystals of the thiocyanate $[(NH_3)_5CoO_2Co(NH_3)_5](SCN)_4$ (notation: $[NH_3]SCN$)[14] were obtained as follows. A 3.75-g sample of $Co(SCN)_2$ was dissolved in 15 mL of H_2O. The solution was filtered and slowly added to 30 mL of 15 M ammonia at 0 °C under stirring. Air was bubbled for 3 h through the solution cooled in an ice bath, and after 1 h 1 g of NH_4SCN was added. Fine needles were collected on a frit and washed with ethanol. A 2-g sample of this material was dissolved in an ice-cold mixture of 30 mL of 15 M NH_3, and the solution was filtered and set aside in a sealed flask at 4 °C. Slow supersaturation was achieved by diffusing thiocyanate through a sealed 3-mL C frit which was filled with 2 g of NH_4SCN dissolved in 2 mL of water and immersed into the saturated solution of the complex. After a few days, needles of up to 5-mm length and 1-2-mm diameter could be collected.

II. $[(en)(dien)CoO_2Co(en)(dien)](ClO_4)_4$. This complex (notation: [en-dien]ClO_4) was prepared according to the literature.[15] Large single crystals were obtained by slow evaporation of the solvent at room temperature.

III. $[(tren)NH_3CoO_2Co(tren)NH_3]^{4+}$. The thiocyanate $[(tren)NH_3CoO_2Co(tren)NH_3](SCN)_4 \cdot 2H_2O$ (notation: $[NH_3$-tren$]SCN$)[16] was prepared by dissolving 0.88 g of $Co(SCN)_2$ in a mixture of 25 mL of H_2O, 25 mL of 15 M NH_3, and 1 g of tren (tris(2-aminoethyl)amine; Aldrich). Air was blown over the solution for 5 min. The solution was then filtered and set aside at room temperature. Supersaturation was achieved by the frit technique described in preparation I. Starting from cobaltous sulfate, $[(tren)NH_3CoO_2Co(tren)NH_3](SO_4)_2 \cdot 6H_2O$ (notation: $[NH_3$-tren$]SO_4$) was obtained. The solution containing the tren ammine complex was set aside in a sealed flask at 4 °C. After a few days, large crystals were collected.

b. Crystal Morphology, Structure, and Molecular Symmetry. Crystal structures of $[NH_3]SCN$,[14] [en-dien]ClO_4,[15] and $[NH_3$-tren$]SCN$[16b] are known. No other structures of simple amine type trans μ-1,2-peroxo cobalt systems exist. For the new systems, $[NH_3]NO_3SCN$ and $[NH_3$-tren$]SO_4$, X-ray structure determinations have been carried out.[17a] Unit cell dimensions as well as space group and morphology are compiled below. The identity of crystals used for spectroscopic work was checked and faces were indexed with a Syntex $P2_1$ four-cycle diffractometer.

$[NH_3]SCN$: orthorhombic, $a = 13.266$ Å, $b = 10.574$ Å, $c = 7.940$ Å, space group *Pnnm*, $Z = 2$;[14] prismatic needles with {110} faces prominent. **$[NH_3]NO_3SCN$**: orthorhombic, $a = 24.327$ Å, $b = 8.170$ Å, $c = 11.174$ Å, space group *Pnma*, $Z = 4$;[17b] crystals similar in shape and size to $[NH_3]SCN$; prominent face {201}. **[en-dien]ClO_4**: monoclinic, $a = 9.062$ Å, $b = 15.981$ Å, $c = 11.153$ Å, $\beta = 92.53°$, space group $P2_1n$, $Z = 2$;[15] prismatic crystals with prominent {011} and {110} faces. **$[NH_3$-tren$]SCN$**: monoclinic, $a = 10.135$ Å, $b = 8.473$ Å, $c = 19.484$ Å, $\beta = 108.58°$, space group $P2_1/c$, $Z = 2$;[16b] crystals in two shapes, either as long needles (up to 2 cm, probably twinned) along *b* with well-developed *bc* faces or as {011} prisms with developed {100} and sometimes {001} faces. **$[NH_3$-tren$]SO_4$**: triclinic, $a = 8.259(2)$ Å, $b = 9.683(4)$ Å, $c = 10.591(3)$ Å, $\alpha = 67.50\ (3)°$, $\beta = 83.65\ (2)°$, $\gamma = 74.57\ (3)°$, space group $P1$, $Z = 1$;[17a] crystals with well-developed {001} and {100} faces.

$[NH_3]SCN$ exhibits the highest possible molecular symmetry for a transplanar cobalt peroxo complex, C_{2h}.[14] Each cobalt ion is surrounded by five nitrogen atoms at distances between 1.947 and 1.971 Å and one oxygen (Co–O distance 1.879 Å) in a nearly octahedral fashion. Bond angles deviate from 90 and 180°, respectively, by less than 2.4°. Six atoms (N–Co–O–O–Co–N) lie in a molecular mirror plane (see Figure 1). Two of the five nitrogens on each cobalt lie above and two lie below this plane, resulting in a "staggered" Co–N configuration with respect to the molecular plane. The halves of the molecule are related by a center of inversion. In $[NH_3]NO_3SCN$, the deviation from O_h symmetry around the cobalt centers is significantly larger with bond angles deviating from 90 and 180° by up to 5.3°; in addition, the center of inversion and the 2-fold rotation axis are lost, resulting in overall C_s molecular symmetry.[17b] The structures of the complex cations are nearly identical

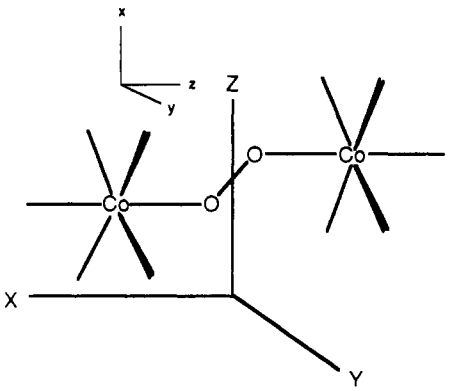

Figure 1. Molecular geometry of trans planar μ-1,2-peroxo cobalt complexes with the molecular coordinate system.

(3) Ross, P. K.; Allendorf, M. D.; Solomon, E. I. *J. Am. Chem. Soc.* **1989**, *111*, 4009.
(4) (a) Baldwin, M. J.; Ross, P. K.; Pate, J. E.; Tyeklar, Z.; Karlin, K. D.; Solomon, E. I. *J. Am. Chem. Soc.* **1991**, *113*, 8671. (b) Pate, J. E.; Ross, P. K.; Thamann, T. I.; Reed, C. A.; Karlin, K. D.; Sorrell, T. N.; Solomon, E. I. *J. Am. Chem. Soc.* **1989**, *111*, 5198. (c) Desjardins, S. R.; Wilcox, D. E.; Musselman, R. L.; Solomon, E. I. *Inorg. Chem.* **1987**, *26*, 288.
(5) (a) Pickens, S. R.; Martell, A. E. *Inorg. Chem.* **1980**, *19*, 15. (b) McLendon, G.; Pickens, S. R.; Martell, A. E. *Inorg. Chem.* **1977**, *16*, 1551.
(6) Bosnich, B.; Poon, C. K.; Tobe, M. L. *Inorg. Chem.* **1966**, *5*, 1514.
(7) (a) Sasaki, Y.; Fujita, J.; Saito, K. *Bull. Chem. Soc. Jpn.* **1969**, *42*, 146. (b) Sasaki, Y.; Fujita, J.; Saito, K. *Bull. Chem. Soc. Jpn.* **1970**, *43*, 3462. (c) Sasaki, Y.; Fujita, J.; Saito, K. *Bull. Chem. Soc. Jpn.* **1971**, *44*, 3373.
(8) Dexter, D. D.; Sutherby, C. N.; Grieb, M. W.; Beaumont, R. C. *Inorg. Chim. Acta* **1984**, *86*, 19.
(9) (a) Lever, A. B. P.; Gray, H. B. *Acc. Chem. Res.* **1978**, *11*, 348. (b) Lever, A. B. P. *Inorganic Electronic Spectroscopy*, 2nd ed.; Elsevier: Amsterdam, 1984; p 285.
(10) Miskowski, V. *Comments Inorg. Chem.* **1987**, *6*, 193.
(11) The only single-crystal spectrum in the literature is severely distorted by scattered-light effects: Yamada, S.; Shimura, Y.; Tsuchida, R. *Bull. Chem. Soc. Jpn.* **1952**, *26*, 72.
(12) Miskowski, V. M.; Santarsiero, B. D.; Schaefer, W. P.; Ansok, G. E.; Gray, H. B. *Inorg. Chem.* **1984**, *23*, 172.
(13) Thewalt, U. *Z. Anorg. Allg. Chem.* **1982**, *485*, 122.
(14) Fronczek, F. R.; Schaefer, W. P.; Marsh, R. E. *Acta Crystallogr.* **1974**, *B30*, 117.
(15) Fritch, J. R.; Christoph, G. G.; Schaefer, W. P. *Inorg. Chem.* **1973**, *12*, 2170.
(16) (a) Zehnder, M.; Fallab, S. *Helv. Chim. Acta* **1972**, *55*, 1691. (b) Thewalt, U.; Zehnder, M.; Fallab, S. *Helv. Chim. Acta* **1977**, *66*, 867.
(17) (a) Tuczek, F.; Musselman, R.; Fronczek, F. R.; Solomon, E. I. To be published. (b) Due to slow decomposition of the crystals of the mixed nitrate–thiocyanate salt of the decaammine peroxo complex in the X-ray beam, structural information on this system is preliminary.

in the $[NH_3\text{-tren}]SO_4$ and $[NH_3\text{-tren}]SCN$ systems.[16,17a] In both systems, the molecules show relatively small variations in Co–N bond lengths (1.95–1.97 Å) but larger deviations from the octahedral 90° (180°) bond angles (maximum 5 and 9°, respectively). The most distorted molecule is $[en\text{-}dien]ClO_4$ with Co–N distances varying between 1.94 and 2.00 Å and bond angles deviating from 90° (180°) by up to 6° (12°).[15] Both the [en-dien] and the $[NH_3\text{-tren}]$ systems, however, retain a center of symmetry, resulting in overall C_i molecular symmetry. The planar Co–O–O–Co configuration and the "staggered" Co–N configuration mentioned above are present in all systems. The structures of the systems included in this study are therefore closely related with an increasing degree of deviation from "ideal" symmetry (monomer, C_{4v}; dimer, C_{2h}) in the order $[NH_3]SCN < [NH_3]NO_3SCN < [NH_3\text{-tren}]SCN = [NH_3\text{-tren}]SO_4 < [en\text{-}dien]ClO_4$.

c. Spectroscopic Measurements. I. Single-Crystal Absorption Spectra. Crystals of cobalt peroxo compounds appear dark brown to black. For single-crystal optical measurements in the UV/vis region, they have to be polished to a thickness of less than 30 μm. In order to achieve a uniform sample thickness and minimize cracking, the crystals were glued with a well-developed face under moderate pressure against an Infrasil (Heraeus Amersil) disk with crystal bond (Arenco products) and ground down to 50–100 μm on an etched glass plate with 10-μm alumina powder. Final machine polishing was achieved with 5-μm alumina powder applied on a polyfoam polishing pad (Rodel, Inc.).

For polarized absorption measurements, the optical properties of the crystal and the crystal morphology have to be taken into account (see below). Only monoclinic $[NH_3\text{-tren}]SCN$ allows a measurement of the crystal spectra along three axes using naturally developed *ab* and *bc* faces. In contrast, $[en\text{-}dien]ClO_4$ does not exhibit useful faces. In this case, samples were obtained by mounting the crystals on a ridge and polishing down the *ab* and *bc* faces. As in the $[NH_3\text{-tren}]SCN$ system, the *b*-axis crystal spectrum common to the two faces was used for normalization of the spectra. Both decaammine systems $[NH_3]SCN$ and $[NH_3]NO_3SCN$ exhibit only one developed face; it was not possible to obtain a second face due to the shape, small size, and mechanical instability of the crystals. For the *ab* and *bc* faces of the triclinic system $[NH_3\text{-tren}]SO_4$, extinction directions were determined with a Vickers M72 polarizing microscope. The "red" absorption direction of the *ab* face was found to make angles of 45 ± 2° with the *b* and 30 ● 2° with the *a* axis, and the "red" absorption direction of the *bc* face was found to make angles of 20 ± 2° with the *b* and 48 ● 2° with the *c* axis. Perpendicular to these directions are the "green" direction of the *ab* face and the "amber" direction of the *bc* face, respectively. By directing a monochromatic beam through the samples mounted in a polarizing microscope we ensured that no dispersion of the indicatrix exists in the visible region.

The crystals were carefully masked off and mounted on a copper sample mount. Optical absorption spectra were obtained with a McPherson RS-10 double-beam spectrometer modified for fully computerized control and data acquisition. The spectrometer is equipped with a McPherson Model 2051 1-m scanning monochromator with predisperser and a Janis Super Varitemp helium cryostat. Spectra in the region between 300 and 800 nm were obtained with a tungsten source, 1200 groove/mm gratings blazed at 300 and 750 nm, and an extended S-20 response photomultiplier tube. The light beam was polarized using a matched pair of Glan-Taylor calcite prism polarizers which have a spectral range of 213 nm–2.3 μm.

II. Glass Spectra. Interpretation of solution spectra of μ-peroxo cobalt complexes is plagued by equilibria with the corresponding doubly bridged species. Samples were therefore prepared by dissolving varying amounts of the complexes in 60:40 mixtures of glycerol/15 M NH_3 at 0 °C, transferring the solution with a syringe between two Infrasil quartz disks mounted in a copper holder, and immediately inserting the holder into an Oxford nitrogen flow cryostat precooled to 80 K. Spectra were obtained on a Cary 17 spectrophotometer interfaced to a Compaq 386 computer with OLIS software. Glass spectra of the decaammine systems invariably showed two bands indicative of practically complete conversion to the doubly bridged species. A clean one-band spectrum was only obtained with $[en\text{-}dien]ClO_4$.

III. Raman Spectra. Crystals of $[NH_3\text{-tren}]SCN$ were ground in an agate mortar and mixed homogeneously with K_2SO_4 (as internal standard) in the ratio 1:5. The $[NH_3]NO_3SCN$ made with $^{16}O_2$ and $^{18}O_2$ was ground and mixed with KBr. The samples were placed in 1 mm i.d. capillary tubes. Resonance Raman spectra were obtained with a Spex 1403 double monochromator and a cooled RCA C31034A photomultiplier combined with a Spex digital photometer system or a Princeton Applied Research Model 1455A intensified diode array detector with a Model 1461 OMA interface. The samples were cooled to approximately 110 K using a nitrogen flow system. A backscattering geometry was employed in light collection. Excessive photodecomposition of the sample had to be prevented in the energy region above 400 nm by using low laser power (down to 10 mW) and short time exposure of the sample to the beam. Single scans were obtained with different sample positions and summed. Error bars correspond to standard deviations of the single scans with respect to the average of 10 scans.

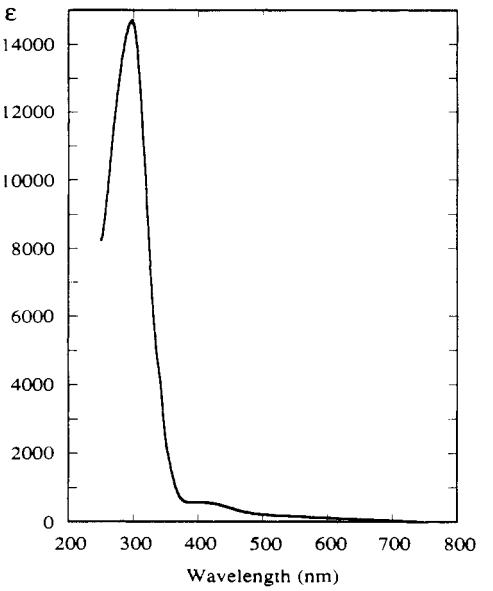

Figure 2. Glass absorption spectrum of $[en\text{-}dien]ClO_4$ at 78 K.

Results

a. Glass Spectra. Figure 2 presents the glass spectrum of $[en\text{-}dien]ClO_4$ at 78 K. The prominent feature is a band at 300 nm with an extinction coefficient of ~14 000 M^{-1} cm^{-1}. Much weaker bands (ϵ <500 M^{-1} cm^{-1}) are observed at 400 and 550 nm. Generally, the solution spectra of monobridged cobalt peroxo complexes are difficult to obtain without interference of the corresponding doubly bridged species. This is particularly evident in the case of the $[NH_3]SCN$ system which exhibits in aqueous solution a spectrum with two bands at 290 and 350 nm, indicative of almost complete conversion to the doubly bridged species. Correspondingly, the lower energy shoulder of the 300-nm band at 350 nm observed in the solution spectra of some monobridged cobalt peroxo complexes is probably associated with the doubly bridged species. In the glass spectrum of the $[en\text{-}dien]ClO_4$ complex (Figure 2), this shoulder is barely visible, indicating that conversion to the doubly bridged species is hindered by the ligand system.

b. Raman Spectra. Raman data have been obtained for $[NH_3]NO_3SCN$ (Figure 3) and $[NH_3\text{-tren}]SCN$. The $[NH_3\text{-tren}]SCN$ system has been used to obtain an excitation profile (Figure 4) as it is more stable toward photodecomposition than the decaammines. In the range between 200 and 1000 cm^{-1}, the $[NH_3\text{-tren}]$ system shows a strong vibration at 800 cm^{-1} whose intensity increases steeply as the excitation wavelength is decreased. Weaker vibrations are observed at 650 and around 500 cm^{-1} (not shown) whose intensities are not significantly dependent upon the excitation wavelength. In the $[NH_3]NO_3SCN$ system, the position of the most intense peak is also found at 800 cm^{-1} and shifts to 750 cm^{-1} upon $^{18}O_2$ substitution (Figure 3, right). The shift of 50 cm^{-1} is consistent with the reduction of the O–O stretching frequency expected from the ratio of the reduced masses of ^{16}O and ^{18}O, respectively. Thus, the 800-cm^{-1} vibration is associated with the O–O stretch. The symmetric Co–O stretch shifts from 650 cm^{-1} with the $^{16}O_2$ compound to 615 cm^{-1} in the $^{18}O_2$ complex (Figure 3, left). In order to obtain more information about the electronic origin of the enhancement of the O–O stretch, the square root of the relative molar frequency-corrected intensity, $(I_J)^{1/2}$,[18] is plotted against the Shorygin function A:

$$A = \frac{1 + (\tilde{\nu}_0/\tilde{\nu}_e)^2}{[1 - (\tilde{\nu}_0/\tilde{\nu}_e)^2]^2} \qquad (1)$$

(18) Clark, R. J. H.; Mitchell, P. D. *J. Mol. Spectrosc.* **1974**, *51*, 458.

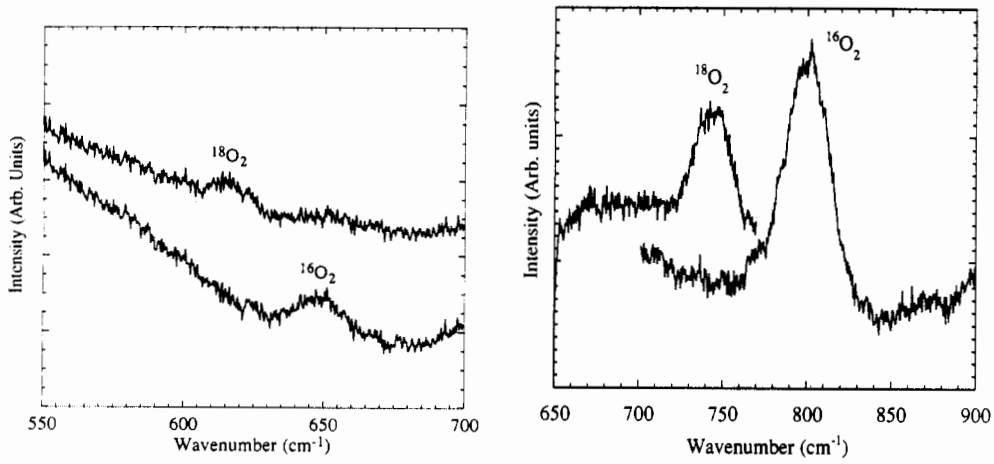

Figure 3. Raman spectrum of $[NH_3]NO_3SCN$ with symmetric Co–O stretch (left) and O–O stretch (right).

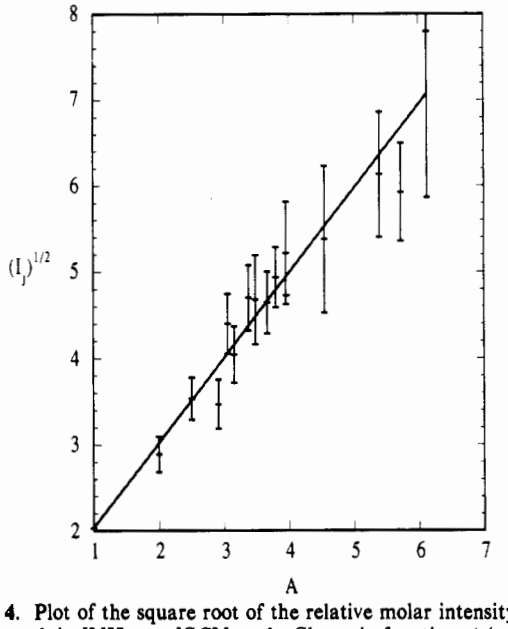

Figure 4. Plot of the square root of the relative molar intensity of the O–O stretch in [NH_3-tren]SCN vs the Shorygin function A (see text).

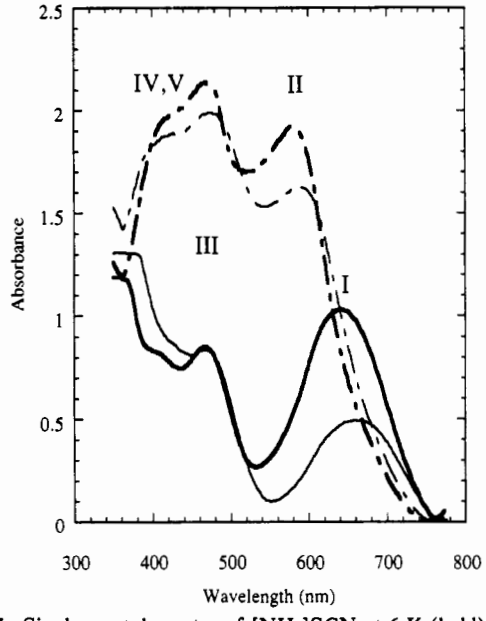

Figure 5. Single-crystal spectra of $[NH_3]SCN$ at 6 K (bold) and 300 K: **E** ∥ c (solid line); E ∥ [110] (dot–dash line).

ν_0 is the excitation frequency. If a totally symmetric mode is enhanced by one specific electronic transition of frequency ν_e, this plot should give a straight line corresponding to an Albrecht A term.[19] Figure 4 shows that this is indeed the case if the 300-nm electronic transition is associated with ν_e.

This result supports the assignment of the 300-nm band as a peroxide to cobalt CT transition. Removal of an electron from the π^* orbitals of peroxide produces a superoxide-like excited state. O–O bond lengths are significantly shorter in superoxides (1.3 Å) than in peroxides (about 1.45 Å[20]); hence, a large change along the nuclear O–O coordinate is expected to be associated with these CT transitions. When bonding to cobalt occurs, the doubly degenerate set of π^* orbitals splits into a π^*_σ and a π^*_ν orbital (see Analysis section). From overlap and energy considerations, the 300-nm band must be the $\pi^*_\sigma \rightarrow$ Co transition. In addition, much weaker transitions are expected from $\pi^*_\nu \rightarrow$ Co at lower energy, which may be visible in the Raman excitation profile of the O–O vibration. However, Figure 4 indicates an enhancement of the O–O stretch with respect to the 300-nm band only. Therefore, the π^*_ν CT transitions either are too weak to cause any deviation from linearity in the A-term behavior of the π^*_σ transition or are at lower energy than 650 nm, which is not probable.[10] The problem of the second CT transition(s) must then be solved with the help of the single-crystal polarized absorption data presented below.

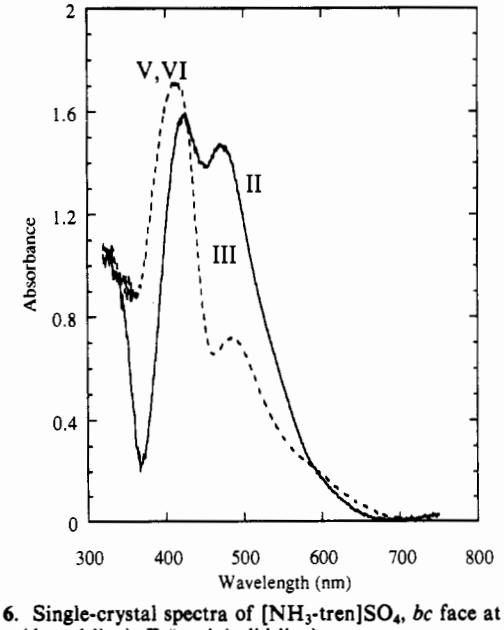

Figure 6. Single-crystal spectra of $[NH_3$-tren$]SO_4$, bc face at 6 K: **E** ∥ amber (dotted line); **E** ∥ red (solid line).

(19) Tang, J.; Albrecht, A. C. In *Raman Spectroscopy*; Szymanski, H., Ed.; Plenum: New York, 1970; Vol. 2, p 33.
(20) See, e.g., ref 1a.

Table I. Band Positions (nm) and Polarizations in Single-Crystal Absorption Spectra

system	face	E ∥	temp	I	II	III	IV	V
$[NH_3]SCN$	{110}	*c*	RT	660,*Z*		475		430,*X*,*Y*(*Z*)
		[110]	RT		590,*X*,*Y*	475		420,*X*,*Y*(*Z*)
		c	6 K	640,*Z*		475		420,*X*,*Y*(*Z*)
		[110]	6 K		580,*X*,*Y*	475		420,*X*,*Y*(*Z*)
$[NH_3]NO_3SCN$	{201}	*b*	175 K	605,*Z*		470		420,*X*,*Y*(*Z*)
		[102]	175 K		540,*X*,*Y*	460		420,*X*,*Y*(*Z*)
$[NH_3$-tren$]SCN$	*ab*	*a*	RT	600,*X*,*Z*		480		435,*X*,*Z*
	bc	*b*	RT	600,*X*,*Z*		500		440,*X*,*Z*
		c	RT		550,*Y*	490	425,*Y*	
	ab	*a*	6 K	610,*X*,*Z*		480		430,*X*,*Z*
	bc	*b*	6 K	600,*X*,*Z*		475		430,*X*,*Z*
		c	6 K		550,*Y*	480	420,*Y*	
$[NH_3$-tren$]SO_4$	*ab*	green	RT	605,*X*,*Z*		475		425,*X*,*Z*
		red	RT		510,*Y*		430,*Y*	
	ab	green	6 K	570,*X*,*Z*		475		425,*X*,*Z*
		red	6 K		510,*Y*		420,*Y*	
	bc	amber	RT			490		420,*X*
		red	RT		500,*Y*		420,*Y*	
	bc	amber	6 K			490		415,*X*
		red	6 K		500,*Y*		420,*Y*	
[en-dien]ClO_4	*ab*	*a*	RT		525,*Y*		435,*Y*	
	bc	*b*	RT	650,*X*,*Z*		500		430,*X*,*Z*
		c	RT		520		430	
	ab	*a*	6 K		525,*Y*		435,*Y*	
	bc	*b*	6 K	630,*X*,*Z*		500		430,*X*,*Z*
		c	6 K		520		430	

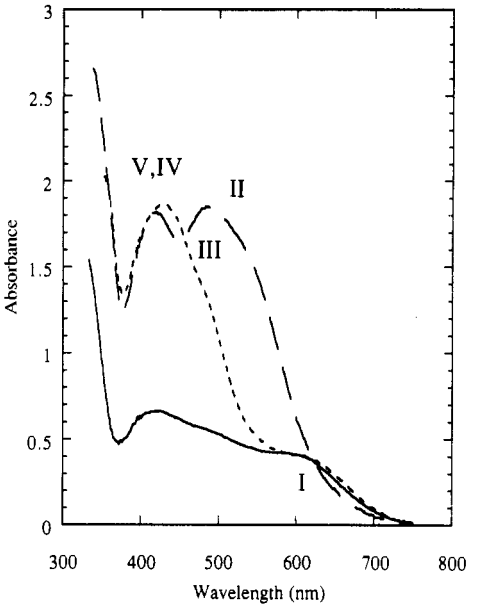

Figure 7. Single-crystal spectra of $[NH_3$-tren$]SCN$ at 6 K: **E** ∥ *b* (solid line); **E** ∥ *a* (dotted line); **E** ∥ *c* (dashed line).

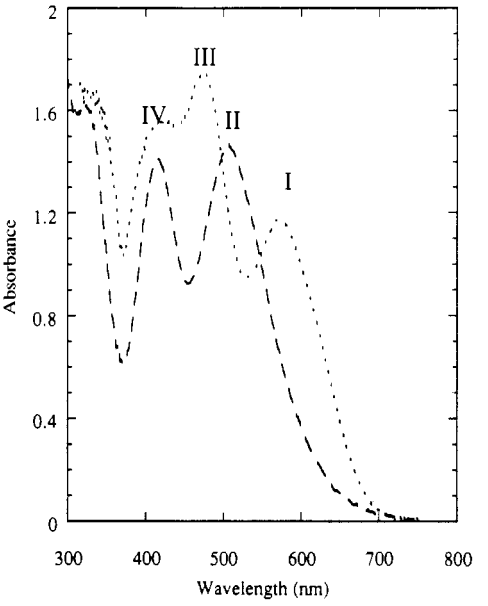

Figure 8. Single-crystal spectra of $[NH_3$-tren$]SO_4$, *ab* face, at 6 K: **E** ∥ green (dotted line); **E** ∥ red (dashed line).

c. Single-Crystal Spectra. Figures 5–9 present the polarized single-crystal absorption spectra of monobridged cobalt peroxo systems. The positions and polarizations of the observed bands as well as the faces and the directions of the electric vector of the light employed in the experiments are compiled in Table I. Note that all spectra correspond to the lower energy absorption region in Figure 2 at wavelengths greater than 350 nm with ϵ values <600 M^{-1} cm^{-1}. Restrictions which apply to the measurement of *crystal* spectra have been presented in the Experimental Section. In order to correlate to molecular selection rules, spectra along *molecular* transition moment directions *X*, *Y*, and *Z* are needed. If the orientation of the molecular coordinate system with respect to the crystal axes *a*, *b*, and *c* is known, the transformation between the set of three crystal spectra along directions *i*,*j*,*k*, ϵ_i, ϵ_j, and ϵ_k, and the set of molecular spectra ϵ_{XX}, ϵ_{YY}, and ϵ_{ZZ} is

$$\begin{pmatrix} \epsilon_i \\ \epsilon_j \\ \epsilon_k \end{pmatrix} = \mathbf{T} \begin{pmatrix} \epsilon_{XX} \\ \epsilon_{YY} \\ \epsilon_{ZZ} \end{pmatrix} \quad (2)$$

with the elements of the transformation matrix **T**, $T_{I,J}$, given by the squared direction cosines of the E vector along $I = i,j,k$ onto the axes $J = X, Y, Z$: $T_{I,J} = \cos^2$ (**I**,**J**). The values $T_{I,J}$ are given in Table II for all crystal systems studied. Note that two possible molecular systems *X*,*Y*,*Z* and *X*′,*Y*′,*Z* have been considered. *X*, *Y*, and *Z* correspond to Figure 1; i.e., *Z* is perpendicular to the Co–O–O–Co plane and *X* is along Co–O. The primed coordinate system is rotated around *Z* with *X*′ directed along the Co–Co vector. The absorption values ϵ_{XX}, ϵ_{YY}, and ϵ_{ZZ} can be considered as principal values of a molecular absorption tensor.[21] If only one of the main axes of the tensor, e.g. *Z*, is known, eq 2 has to be replaced by a more general expression involving ϵ_{XY} in addition to ϵ_{XX}, ϵ_{YY}, and ϵ_{ZZ}. Therefore, four measurements are required to determine the absorption tensor, which may then be diagonalized, giving the desired principal directions and values. If none of the axes *X*,*Y*,*Z* is known, six measurements are required to obtain this information.

(21) (a) Hitchman, M. A. *J. Chem. Soc., Faraday Trans. 2* **1976**, *72*, 54. (b) Hitchman, M. A. In *Transition Metal Chemistry*; Melson, G. A., Figgis, B. N., Eds.; Dekker: New York, 1985; Vol. 9, p 1.

Table II. Crystal Faces and Molecular Projections (%) with $X \parallel$ Co–O ($X' \parallel$ Co–Co) and $Z \perp$ Co–O–O–Co

system	face	E ∥	X	X′	Y	Y′	Z
$[NH_3]SCN$	{110}	[110]	54.92	48.18	45.08	51.82	0
		c	0	0	0	0	100
$[NH_3]NO_3SCN$	{201}	[102]	51.97	49.50	48.03	50.50	0
		b	0	0	0	0	100
[en-dien]ClO_4	*ab*	*a*	19.27	2.35	73.00	89.92	7.73
	bc	*b*	43.45	43.10	0.92	1.27	55.63
		c	39.61	55.45	22.32	6.49	38.07
$[NH_3$-tren]SCN	*ab*	*a*	51.22	27.83	25.02	48.41	23.76
	bc	*b*	12.14	5.04	12.19	19.29	75.67
		c	11.95	37.04	82.91	57.82	5.15
$[NH_3$-tren]SO_4	*ab*	green	28.15	21.87	1.45	7.73	70.40
		red	13.14	0.62	74.45	86.94	12.44
	bc	amber	87.83	92.54	5.22	0.50	6.69
		red	10.93	0.37	67.72	78.29	21.34

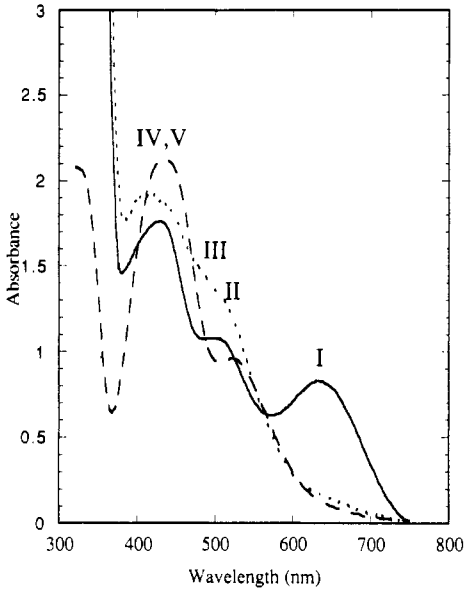

Figure 9. Single-crystal spectra of [en-dien]ClO_4 at 6 K: **E** ∥ *a* (dashed line); **E** ∥ *b* (solid line); **E** ∥ *c* (dotted line).

The highest symmetry system is $[NH_3]SCN$. Since the molecular symmetry is C_{2h}, electronic polarizations either are in the molecular plane or are perpendicular to it. Transitions within the plane defined by the Co–O–O–Co framework are designated *X,Y* polarized; those perpendicular to it are *Z* polarized (see Figure 1). The X-ray structure shows *Z* to coincide with *c*.[14] The *Z* (**E** vector parallel to *c*) spectrum (Figure 5, solid lines) shows three bands whose positions are given in Table I. The lowest energy band at 660 nm (640 nm at 6 K) is referred to as band I ($\epsilon \approx 100\ M^{-1}\ cm^{-1}$). In contrast, the spectrum with **E** along [110] (Figure 5, dot–dash) is of mixed character (see Tables I and II). It contains three bands (see Table I) with the band at 590 nm referred to as band II. Obviously, band I appears only out-of-plane (*Z*) and band II only in-plane (*X,Y*). Note that the intensity of band I increases by a factor of 2 if the temperature is lowered from 300 to 6 K and that its position shifts to higher energy. It will be shown below that two transitions corresponding to bands IV and V coincide in the band at 430 nm (420 nm at 6 K). The in-plane *X,Y* intensity is larger than the out-of-plane *Z* intensity, which is denoted by *X,Y*(*Z*) in Table II. This also applies to band III at 475 nm.

The second decaammine salt, $[NH_3]NO_3SCN$, provides similar information (data not shown). In this case, the molecular symmetry is C_s. A pure *Z*-polarized spectrum is observed along *b*. The in-plane spectrum (**E** parallel to [102]) is again of mixed *X,Y* character (see Table II). As in $[NH_3]SCN$, band I is out-of plane (*Z*) and band II in-plane (*X,Y*) polarized. Since the composition of the in-plane spectra in terms of molecular contributions is very similar to that of $[NH_3]SCN$ (see Table II) and a second face is not available, it is not possible to decompose the in-plane spectrum into its *X* and *Y* contributions. The two $[NH_3$-tren] systems are used below to obtain this information.

The X-ray structures of $[NH_3$-tren]SCN and $[NH_3$-tren]SO_4 show that the complex cations are nearly identical in both salts (see Experimental Section); hence, very similar molecular spectra are expected. In both cases, the molecular symmetry is C_i, which imposes no restriction on the orientation of the *X,Y,Z* transition moment system. Due to the close structural similarity with the higher symmetry decaammine cobalt peroxo cation, however, effective C_s (or C_{2h}) symmetry is assumed, which fixes *Z* in a position normal to the Co–O–O–Co plane. We must then determine the orientation of *X* and *Y* within this plane. According to the above considerations, four independent measurements are generally required for this case. Since this information cannot be obtained from the available crystal faces, we cannot solve the problem rigorously. However, the two reasonable orientations for one of the in-plane axes are parallel to the Co–O vector (*X*; cf. Figure 1) and parallel to the Co–Co vector (*X′*). Table II gives the decomposition of all spectra in terms of contributions along *X,Y,Z* and *X′,Y′,Z* (see eq 2). The cleanest spectrum is the amber $[NH_3$-tren]SO_4 *bc* face spectrum (Figure 6, dotted), which contains a high contribution of *X* (88%) as well as *X′* (93%). It shows a dominant band at 420 nm (415 nm at 6 K), which is designated as band V. In addition, a weaker band (band III) is present at 490 nm, which corresponds to the 475-nm band of the $[NH_3]SCN$ system. Three spectra of high *Y* or *Y′* character are the $[NH_3$-tren]SCN *c* spectrum (Figure 7, dashed; 83% *Y*, 58% *Y′*), the red $[NH_3$-tren]SO_4 *ab* face spectrum (Figure 8, dashed; 74% *Y*, 87% *Y′*), and the red $[NH_3$-tren]SO_4 *bc* face spectrum (Figure 6, solid; 68% *Y*, 78% *Y′*). The first two appear very similar, which is reflected satisfactorily by the *X,Y,Z* coordinate system (12% *X*, 83% *Y*, 5% *Z* for the *c* spectrum and 13% *X*, 75% *Y*, 12% *Z* for the red *ab* face spectrum). In contrast, the primed system is not consistent with the similarities (37% *X′*, 58% *Y′* vs 1% *X′*, 87% *Y′*). *Therefore, the in-plane molecular polarizations are given by the unprimed coordinate system X,Y with X along the Co–O bond.* Band II appears in the $[NH_3$-tren] spectra of high *Y* character, but not in the spectra of high *X*, i.e. the amber *bc* face spectrum of $[NH_3$-tren]SO_4 (Figure 6, dotted), and high *X,Z* character, i.e. the *a* spectrum of $[NH_3$-tren]SCN (Figure 7, dotted); therefore, it is *Y* polarized. All spectra of high *Y* character show a second band at higher energy (420–435 nm; see Table I), which is designated band IV. Since the spectra of high *X* character are dominated by band V at about the same energy position (see above), the 425-nm in-plane band of the decaammine systems is composed of two bands of *X* and *Y* polarization.

The *b* spectrum of $[NH_3$-tren]SCN (Figure 7, solid line), which contains 76% *Z*, is less intense than the *a* (24% *Z*) and *c* (5% *Z*) spectra, in agreement with the $[NH_3]SCN$ case. However, band I, which was purely *Z* polarized in $[NH_3]SCN$, is present with equal intensity in the *b* and *a* (dotted; 24% *Z*, 51% *X*, 25% *Y*) spectra. Since it is not present in the *c* spectrum (dashed; 83% *Y*), its polarization is *X,Z* in the $[NH_3$-tren] salt. It appears that, due to the lower symmetry of the $[NH_3$-tren] system, the *Z* axis of the absorption tensor for band I is rotated around *Y* toward *X*. This observation is supported by crystal spectra of [en-dien]ClO_4 (Figure 9). The crystal axes are nearly orthogonal (α

$= \gamma = 90°$, $\beta = 92.53°$ [15]). Band I is cleanly polarized along *b* (solid line; 56% *Z*, 43% *X*, 1% *Y*), i.e. along a direction between *Z* and *X*. Its intensity increases with lower temperature, and its position moves to higher energy (see Table I). Band II at 525 nm (520 nm at 6 K) is not present in this spectrum, in agreement with its vanishing *Y* contribution (1%). In contrast, it appears in the *a* spectrum at 520 nm (6 K) (dashed; 73% *Y*), lending support to its earlier *Y* polarization assignment. In agreement with the data for both [NH_3-tren] salts, the *a* spectrum contains a second *Y*-polarized band, band IV, at 420 nm (6 K). Band V is present in the *b* spectrum of mixed *X*/*Z* character at 430 nm (6 K).

To summarize, *band I* at 650 nm has been determined to be *Z* polarized in [NH_3]SCN and *X*,*Z* polarized in lower symmetry (C_i) systems. *Band II* is *Y* polarized, and *bands IV* and *V* have been determined to be *Y* and *X* polarized, respectively. *Band III* appears in all polarizations. Its position is rather constant at 475–500 nm. In [NH_3]SCN and [en-dien]ClO_4, the intensity of band I increases at low temperatures whereas the intensities of all other bands slightly decrease. Further, the position of band I shifts to higher energy whereas no shifts are observed for the other bands. These observations indicate that band I is more sensitive to low-symmetry distortions of the complex than the other bands (vide infra).

Assignments and Analysis

Optical spectra of the cobalt peroxo complexes have been interpreted by comparison to those of the monosubstituted or trans-disubstituted cobalt hexaammines.[5,6] We refer to Figure 10A in the following analysis.[22] The octahedral complex $[Co(NH_3)_6]^{3+}$ shows two prominent bands in the ligand field (LF) region: the first at 21 050 cm^{-1} (ϵ = 60 M^{-1} cm^{-1}) corresponds to the $^1A_1 \rightarrow {}^1T_1$ transition; the second one at 29 500 cm^{-1} (ϵ = 55 M^{-1} cm^{-1}), to the $^1A_1 \rightarrow {}^1T_2$ transition.[23] These transitions are one-electron transitions from the filled t_{2g} octahedral manifold to the empty e_g manifold. Upon removal of one NH_3 ligand, the energy of the z^2 orbital is lowered with respect to the *xy* orbital and the energy of the *xz*, *yz* orbitals is lowered with respect to the $x^2 - y^2$ orbital (Figure 10A, left). Bonding of an axial ligand other than NH_3 (e.g. halide or peroxide) results in a shift of the z^2 orbital to higher energy depending on the strength of σ antibonding (Figure 10A, middle). In general, the π-antibonding effect of the ligand orbitals must also be considered. The Co *xy* and $x^2 - y^2$ orbitals, lying in a plane perpendicular to the substituent, are not affected by changes in either axial π or σ bonding. This is well-documented experimentally[24] and used below. The $^1T_1$ transition in $[Co(NH_3)_6]^{3+}$ is at 475 nm (see above), whereas the $^1A_2(x^2 - y^2 \rightarrow xy)$ component of the $^1T_1$ transition in the mono-substituted or trans-disubstituted hexaammines is at 455–475 nm. The *xz* and *yz* orbitals, in contrast, may be subject to a π-antibonding interaction, resulting in a shift of the corresponding transitions to the e_g orbitals to lower energy. In fact, these transitions (the $^1E^a$ *xz*, *yz* $\rightarrow$ *xy* component of $^1T_1$) are observed at 510–580 nm in monosubstituted and 580–660 nm in trans-disubstituted hexaammines and are the lowest energy singlet transitions in these systems. Note that configuration interaction between various low-symmetry-split strong-field states has not been included in estimating this qualitative energy ordering.

There is an important difference between bonding in halo pentaammines and bonding in peroxo complexes (see Figure 10A, right and middle): the doubly degenerate highest occupied molecular orbital of peroxide, π^*, splits into two nondegenerate MO's upon bonding to cobalt, one σ-bonding π^*_σ within the Co–O–O–Co plane and one π-bonding orbital π^*_v vertical with respect to the plane. This reduces the effective symmetry of the monomer site to C_{2v}, splits the *xz* and *yz* orbitals, and removes all degeneracy of the T_1 and T_2 excited states. π bonding occurs only between

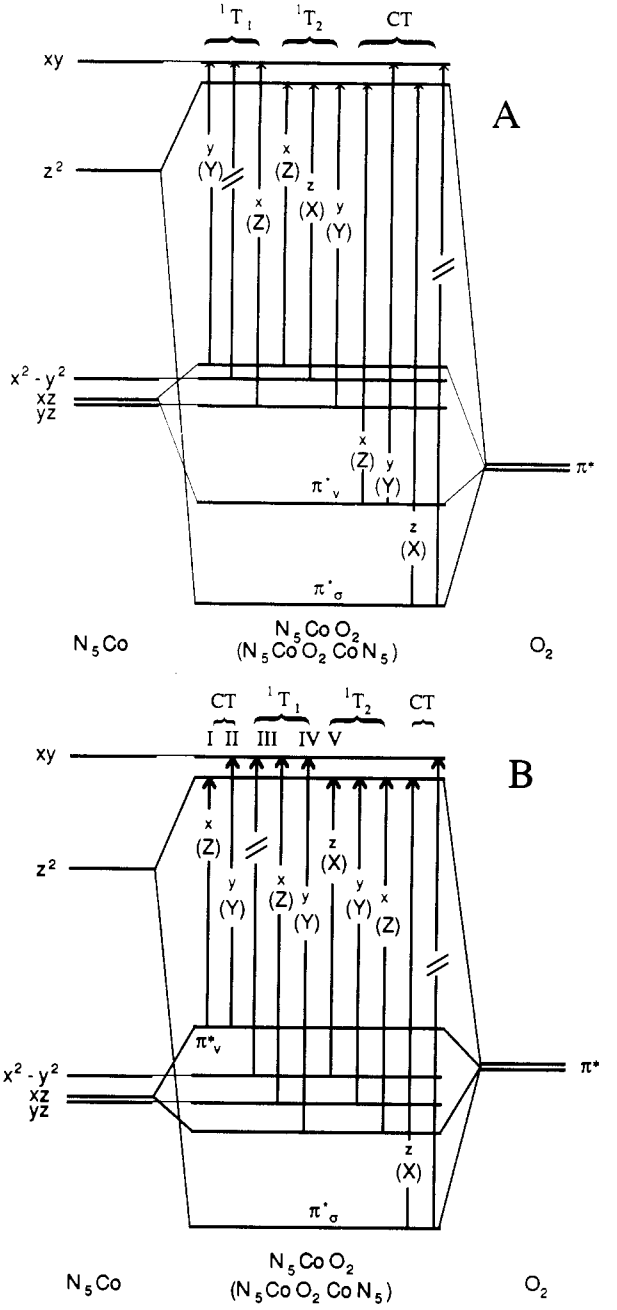

Figure 10. (A) Bonding scheme of cobalt peroxo complexes with $\pi^*(O_2^{2-})$ lower than the metal t_{2g} orbitals, polarizations in monomer (lowercase) and dimer (uppercase). (B) Bonding scheme for the same complexes with $\pi^*(O_2^{2-})$ higher than the metal t_{2g} orbitals.

xz and π^*_v, and σ bonding occurs between z^2 and π^*_σ. According to the previous considerations, the $x^2 - y^2 \rightarrow xy$ ($^1A_2$) transition should shift little with respect to the parent $^1T_1$ transition. The transitions corresponding to $^1A_1 \rightarrow {}^1E^a$ in the halo pentaammines, on the other hand, should split depending on the strength of the π-antibonding effect of π^*_v. The *xz* $\rightarrow$ *xy* transition should shift to lower energy and become the lowest energy LF transition, and the *yz* $\rightarrow$ *xy* transition should shift very little (Figure 10A, middle).

So far, only electronic states and transitions centered on the monomer subunits have been considered. To obtain dimer states, a coupled-chromophore approach is adopted.[25] Evaluation of the electric dipole transition operator between the dimer ground and excited states shows that single-site transition moments add or subtract in the dimer ("transition dipole vector coupling"). Since one component of each combination is not electric dipole allowed, a 1:1 correlation exists between monomer (single-site) and dimer

(22) Note that the coordinate system of Figure 1 interchanges $x^2 - y^2$ with *xy* and $(xz + yz)$, $(xz - yz)$ with *xz*, *yz*.
(23) Wilson, R. B.; Solomon, E. I. *J. Am. Chem. Soc.* **1980**, *102*, 4085.
(24) Wentworth, R. A. P.; Piper, T. S. *Inorg. Chem.* **1965**, *4*, 709.
(25) Hansen, A. E.; Ballhausen, C. J. *Trans. Faraday Soc.* **1965**, *61*, 631.

transitions. The monomer (lowercase) and dimer polarizations (uppercase, in parentheses) are included in Figure 10A. The correspondence between the monomer and the dimer coordinate systems is shown in Figure 1. Figure 10A also indicates the polarizations of the CT transitions. π^*_σ bonding to the Co z^2 orbital along the X axis is the dominant bonding interaction of peroxide; correspondingly, there is good overlap between these orbitals and the intensity of the $\pi^*_\sigma \rightarrow Co(z^2)$ CT band is very high. The $\pi^*_\sigma \rightarrow Co(xy)$ transition is forbidden. Overlap between the π^*_v and the Co z^2 and xy orbitals is zero, and thus the $\pi^*_v \rightarrow$ metal transitions should have very little intensity.

The bonding scheme of Figure 10A implies that the lowest energy LF transition from the xz orbital (which is π antibonding to O_2^{2-}) to the xy orbial is Y polarized in the dimer. Band I, which is observed at 660 nm in $[NH_3]SCN$, however, is Z polarized (the X,Z polarization observed in the lower symmetry systems will be commented on below). Figure 10A shows that candidates for a Z-polarized transition are $yz \rightarrow xy$ ($^1T_1$), $xz \rightarrow z^2$ ($^1T_2$), and $\pi^*_v(O_2^{2-}) \rightarrow z^2$. The second possibility can be excluded, as transitions of $^1T_2$ parentage cannot be at this low an energy (see below). The first possibility is also not reasonable, as both orbitals involved are nonbonding and thus the electronic transition between them cannot shift to much lower energy than found for the $^1T_1$ parent transition (see above). *Band I* must therefore be assigned to the $\pi^*_v(O_2^{2-}) \rightarrow z^2$ CT transition, which could not be detected in the resonance Raman experiment due to its low intensity ($\epsilon \approx 100\ M^{-1}\ cm^{-1}$). This assignment, however, requires the bonding scheme in Figure 10A to be reversed from its conventional order; i.e., $\pi^*_v(O_2^{2-})$ is now higher in energy than the filled t_{2g} metal orbitals (Figure 10B). Since in this scheme xz is involved in a bonding interaction with π^*_v, the Y-polarized transition from xz to xy, predicted to be the lowest energy transition of $^1T_1$ parentage in Figure 10A, should now become the highest energy transition of $^1T_1$ parentage in Figure 10B. *Band IV* of Y polarization is assigned to this transition. *Band II*, which is also Y polarized and 1800 cm^{-1} above band I in $[NH_3]SCN$, is associated with the second CT from $\pi^*_v(O_2^{2-})$ to xy. The remaining transition of Y polarization, $yz \rightarrow z^2$ ($^1T_2$), is higher in energy and probably masked by the $\pi^*_\sigma(O_2^{2-}) \rightarrow z^2$ CT band at 300 nm. The only transition predicted to be of X polarization besides the intense $\pi^*_\sigma \rightarrow z^2$ transition is $x^2 - y^2 \rightarrow z^2$ ($^1T_2$), which is assigned to *band V*. Transitions of $^1T_2$ character have been observed in other substituted Co ammines at this energy.[26] The Z (out-of-plane) intensity at 475 nm, *band III* in $[NH_3]SCN$, may be attributed to $yz \rightarrow xy$ ($^1T_1$), the separation to $xz \rightarrow xy$ (Y) at 425 nm (2500 cm^{-1}) being a measure for the π-bonding effect (see Figure 10B, middle). Band III, however, also has in-plane intensity in all systems. As with bands IV and V at 425 nm, band III appears to be associated with two different transitions. On the basis of its energy, the band at 475 nm would correspond to the $x^2 - y^2 \rightarrow xy$ transition, since the corresponding $^1A_2$ transition of the substituted cobalt ammines is found at 455–475 nm and shows little dependence on the substituent (see above). Since $x^2 - y^2 \rightarrow xy$ is formally forbidden, low-symmetry distortions (static or vibronic) are required to explain the observed in-plane intensity.

Finally, the polarization and energy behavior of band I requires further consideration. In $[NH_3]SCN$ its intensity along the Z direction increases and its position shifts from 660 to 640 nm as the temperature is lowered from 300 to 6 K (Figure 5). These effects are not present in the other bands. As indicated above, the $\pi^*_v(O_2^{2-}) \rightarrow$ Co CT transitions are expected to have no intensity due to vanishing overlap although they are group-theoretically allowed. The fact that the $\pi^*_v(O_2^{2-}) \rightarrow$ Co CT transitions are observed at room temperature can be attributed to intensity stealing from strongly allowed CT transitions. This mechanism, however, should not be temperature dependent and cannot account for the intensity increase of band I upon lowering the temperature. This must involve a temperature-dependent distortion of the molecule, which causes a nonvanishing overlap between the $\pi^*_v(O_2^{2-})$ and Co z^2 and xy orbitals and thereby increases the intensity of the corresponding CT transitions. It is not clear whether this distortion, which requires a symmetry reduction from the C_{2v} point group at room temperature, is caused by sample strain induced by cooling or a crystallographic phase transition. Since the Co z^2 orbital is directed toward the oxygen atoms and the xy orbital is in a plane perpendicular to the Co–O bond, the intensity of the $\pi^*_v \rightarrow z^2$ transition (band I) is predicted to be increased more strongly than the intensity of the $\pi^*_v \rightarrow xy$ transition (band II), in accordance with the observation.

In $[NH_3$-tren$]SCN$ and [en-dien]ClO_4, a rotation of the transition moment vector of band I toward the Co–O axis is observed. For these molecules the symmetry of the complex is C_i, allowing some mixing of the peroxide π^*_σ and π^*_v orbitals. This gives the $\pi^*_v \rightarrow z^2$ transition (Z polarized) some $\pi^*_\sigma \rightarrow z^2$ (X polarized) character and results in a transition moment direction between Z and X. In addition, the $\pi^*_v \rightarrow z^2$ transition (band I) is expected to shift to higher energy as π^*_σ is admixed. The shift of band I observed in [en-dien]ClO_4 from 650 nm (300 K) to 630 nm (6 K) must therefore be due to an increased contribution of π^*_σ at low temperature. In contrast to the $[NH_3]SCN$ system, no symmetry reduction of the molecule is necessary for this effect. The assignments of the excited states of trans μ-1,2-peroxo cobalt complexes are summarized in Table III.

Table III. Assignments of the Electronic Transitions of Trans μ-1,2-Peroxo Cobalt Complexes

band	energy range, nm	polarizn	assgnt	remarks
I	660–570	Z	$\pi^*_v \rightarrow z^2$	rotation toward X
III	590–500	Y	$\pi^*_v \rightarrow xy$	
III	500–475	X, Y	$x^2 - y^2 \rightarrow xy$	formally forbidden
		Z	$yz \rightarrow xy$	
IV	420–435	Y	$xz \rightarrow xy$	
V	415–440	X	$x^2 \rightarrow y^2 \rightarrow z^2$	
	300	X	$\pi^*_\sigma \rightarrow z^2$	

Discussion

The single-crystal polarized absorption data for the trans μ-1,2-peroxo cobalt complexes presented in this study allow an assignment of the $\pi^*_v(O_2^{2-}) \rightarrow d\sigma(Co)$ charge-transfer (CT) transitions, which have been the subject of much speculation.[5,9,10] In accordance with the limited overlap between the metal $d\sigma$ and ligand π^*_v orbitals, the intensity of these transitions is low ($\epsilon \approx 100\ M^{-1}\ cm^{-1}$). More importantly, band I and band II, which are assigned to $\pi^*_v(O_2^{2-}) \rightarrow z^2(Co)$ and $\pi^*_v(O_2^{2-}) \rightarrow xy(Co)$ CT, respectively, are found to be at lower energy than the ligand field transitions (bands III–V). Therefore, the highest occupied molecular orbital (HOMO) in trans μ-1,2-peroxo cobalt complexes has ligand π^*_v character. This parallels the bonding scheme of trans μ-1,2-superoxo cobalt complexes (see below). In most of the substituted cobalt hexaammines, the HOMO has metal character. Therefore, band I, which has been observed in solution spectra of monobridged cobalt peroxo systems, has been previously assigned as a LF transition.[5a,6]

The ligand field bands (bands III–V) appear at energies typical for Co(III) systems. Their shifts and splittings reflect the coordination to a ligand with one π orbital perpendicular to the molecular Co–O–O–Co plane. Thus, the $^1A_1 \rightarrow {}^1E^a$ transition, which is at lower energy than the $^1A_1 \rightarrow {}^1A_2$ transition in most monosubstituted cobalt ammine systems, is split by 2500 cm^{-1} and shifted to higher energy. Dimer interactions split the transitions into g and u combinations due to the inversion symmetry of the complexes. As only transitions from the $^1A_{1g}$ ground state to u excited states are electric dipole allowed, dimer splittings are not experimentally observed.

The results of the Raman experiments are supported by literature data. Vibrational frequencies have been determined for a number of monobridged trans μ-1,2-peroxo cobalt systems.[27,28]

(26) Dingle, R. *J. Chem. Phys.* **1967**, *46*, 1.

(27) (a) Shibahara, T.; Mori, M. *Bull. Chem. Soc. Jpn.* **1978**, *51*, 1374. (b) Barraclough, C. J.; Lawrance, G. A.; Lay, P. A. *Inorg. Chem.* **1978**, *17*, 3317. (c) Freedman, T. B.; Yoshida, C. M.; Loehr, T. M. *J. Chem. Soc., Chem. Commun.* **1974**, 1016.

Peaks around 800 and 640 cm^{-1} have been assigned to the intra-peroxide and symmetric Co–O stretch, respectively.[27] The data on simple decaammine salts[27] are confirmed by our isotope shifts. Freedman et al. have noticed a large intensity increase of the O–O peak as the excitation wavelength is decreased.[27] This results from the Franck–Condon A term behavior of the O–O stretch (Figure 4) with respect to the intense 300-nm band and supports the earlier assignment of this band as a $\pi^*_\sigma(O_2^{2-}) \rightarrow d\sigma(Co)$ charge-transfer transition.[27] In monobridged cobalt peroxo salen systems (salen = *N*,*N*′-ethylenebis(salicylideneamine)), where this CT transition is at lower energy, e.g. [BCo(salen)O_2(salen)CoB] (B = DMF, pyridine *N*-oxide), the O–O vibration enhancement profile reflects the band shape.[28] In contrast, Co–O stretch peak intensity is low at all excitation wavelengths, indicating that it is not significantly enhanced with respect to the 300-nm band. This parallels the behavior for the Cu–O stretch observed in the $\pi^*_\sigma(O_2^{2-}) \rightarrow$ Cu(II) CT transition in a trans planar μ-1,2-peroxo copper complex[4a] (see below). In the copper peroxide system, however, the $\pi^*_v \rightarrow$ Cu transition has significant absorption intensity, and strong enhancement of the Cu–O vibration peak intensity with respect to $\pi^*_v \rightarrow$ Cu is observed. The lack of enhancement of the Cu–O stretch with respect to the π^*_σ CT and the enhancement with respect to the π^*_v CT transition have been attributed to the fact that π^*_σ is delocalized over the two copper centers, which results in distortions that are very different than predicted for a peroxide–metal monomer. In contrast, π^*_v is localized and monomer-like excitation behavior is observed. The different degree of delocalization of the two CT excited states has been supported by broken-symmetry SW–Xα calculations.[4a]

The results obtained in a detailed spectroscopic study of a superoxo complex[12] can now be related to those of analogous peroxo systems. The complex studied, $[(NH_3)_5CoO_2Co(NH_3)_5](NO_3)_2Cl_3{\cdot}2H_2O$, is structurally closely related to the cobalt decaammine peroxo systems investigated here. In contrast to the case of the peroxo systems, the π^*_v orbital is now singly occupied and a MLCT transition from the metal dπ orbitals to $\pi^*_v(O_2^-)$ is observed at 680 nm. This places the π^*_v orbital at higher energy than the metal dπ manifold, which corresponds to the bonding scheme derived here for the peroxo systems. LF transitions of $^1T_1$ character are assigned at 480 nm (X polarized; $^1A_1 \rightarrow {}^1E^a$) and 464 nm ($Z$ polarized; $^1A_1 \rightarrow {}^1A_2$) on the basis of vibronic selection rules. These assignments are not consistent with those of cobalt peroxo systems, since the ^1E transitions appear at lower energy than the $^1A_1$ transition and they do not split. The latter observation indicates a local tetragonal (C_{4v}) symmetry. It appears that, in contrast to the case of the cobalt peroxo systems, the effect of the low-energy π^*_v orbital on the metal dπ orbitals is not significant. The $\pi^*_\sigma \rightarrow$ Co CT transition is observed at 300 nm in the superoxo systems, consistent with the cobalt peroxo systems, indicating there is a similar stabilization of the π^*_σ orbital. No definitive assignment is made for the $\pi^*_v \rightarrow$ Co CT transition in the superoxo system.

Our results may be related to the cis-dibridged cobalt peroxo systems. Their optical spectra display intense bands at ~290 and ~350 nm,[9,10] in contrast to the optical spectra of trans planar μ-1,2-peroxo cobalt complexes, which show only one strong band at 300 nm (Figure 2). Both bands of the cis complexes have approximately the same intensity (ϵ = 5000–7000), which is about half the value for the 300-nm band of the monobridged complexes. X-ray structures show that the dibridged peroxo complexes have dihedral angles around 60°.[1] It is generally believed that the differences between the spectral features of the monobridged and dibridged complexes are due to the bending of the Co–O–O–Co bridge out of the plane.[9,10] This mixes the set of $\pi^*_v(O_2^{2-})$ and $\pi^*_\sigma(O_2^{2-})$ orbitals, which diminishes the intensity differences of the corresponding LMCT transitions and shifts the energies of the transitions toward each other. A scheme has been proposed which accounts for the shifting of the CT bands as a function of the dihedral angle Θ.[10] Our results on trans planar μ-1,2-peroxo cobalt systems show evidence for these orbital mixing effects arising from small distortions of a planar peroxide configuration. It has been noted that the 290-nm band of the doubly bridged complexes does not fit this explanation, since its energy is higher than that of the $\pi^*_\sigma(O_2^{2-}) \rightarrow$ Co transition in the planar systems, and that the assignment to a charge transfer from the bridging amide or hydroxide to the cobalt may be more reasonable.[10]

Assignment of the lowest energy band (band I) as the $\pi^*_v(O_2^{2-}) \rightarrow z^2$ CT transition has important implications with respect to the photochemistry of cobalt peroxo complexes. Maecke et al. find the main photoreaction for mono- and dibridged cobalt peroxo compounds in aqueous solution to be photoinduced deoxygenation.[29] The wavelength dependence, however, is drastically different for mono- and dibridged systems: whereas the monobridged complex $[(papd)CoO_2Co(papd)]^{4+}$ (papd = 1,5,8,11,15-pentaazapentadecane) releases oxygen upon irradiation at a yield of ca. 3.5×10^{-2} independent of the excitation wavelength in the range of 297–546 nm, the doubly bridged systems show a clear correlation of the rate of oxygen release with the band at 290 nm. For example, for $[(tren)Co(O_2,OH)Cotren]^{3+}$ the quantum yield increases from 0.6×10^{-3} at 435 nm to 1.9×10^{-2} at 300 nm. Maecke explains these differences by invoking a low-lying ($\lambda > 546$ nm) $\pi^*_v \rightarrow z^2$ CT excited state in the monobridged complex. Our assignment of the lowest energy band, band I, to this CT transition proves this assumption to be valid. The transfer of an electron from an antibonding (with respect to the O–O bond) ligand orbital to an antibonding (with respect to the Co–O bond) metal orbital weakens the Co–O bond and strengthens the O–O bond. Splitting the Co–O bond should then result in a mononuclear $Co^{III}O_2^-$ superoxo fragment of O_2^- $(\pi^*_\sigma)^2(\pi^*_v)$ configuration and a reduced Co^{II} species. The superoxo species may further decay with release of dioxygen. It is important that once this $\pi^*_v \rightarrow z^2$ CT excited state is populated, the photoinduced reaction can take place. Obviously, the excitation energy must be above a threshold determined by the energy of band I. Maecke points out that transfer of an electron from the π^*_σ orbital is ineffective, since the resulting electronic configuration, $(\pi^*_\sigma)(\pi^*_v)^2$, is unfavorable for the formation of a $Co^{III}O_2^-$ fragment. Hence, no increase of quantum yield of photoinduced O_2 release is observed with respect to the 300-nm band. This is in contrast to the photochemical behavior of the corresponding monobridged superoxo systems. Here, the $\pi^*_\sigma \rightarrow z^2$ transition produces triplet oxygen, $(\pi^*_\sigma)(\pi^*_v)$; hence, a clear correlation of the rate of photoinduced O_2 release with the 300-nm band is observed.

Recently, an optical and resonance Raman spectroscopic study of the trans μ-1,2-peroxo-bridged binuclear copper complex has been carried out.[4a] The overall point group symmetry of the dimer is C_i, while the Cu_2O_2 unit has C_{2h} symmetry. The coordination geometry around each copper center is close to trigonal bipyramidal with significant overlap between the half-occupied dz^2(Cu) and $\pi^*_\sigma(O_2^{2-})$ orbitals. There are two striking differences in the CT spectra of the trans μ-1,2-peroxo copper dimer and the analogous cobalt dimer: (i) Whereas the intensities of the $\pi^*_v(O_2^{2-}) \rightarrow$ Co CT transitions are small and comparable to that of allowed ligand field bands, the $\pi^*_v(O_2^{2-}) \rightarrow$ Cu CT transition is more than an order of magnitude more intense and comparable to the $\pi^*_\sigma(O_2^{2-}) \rightarrow$ Cu CT intensity. The $\pi^*_\sigma \rightarrow$ metal transition, however, has similar intensity in both dimers. (ii) The separation between the spin-allowed CT bands is 17 000 cm^{-1} for the cobalt complex and only 2600 cm^{-1} for the copper complex. The high intensity of the π^*_v CT band in the copper dimer is explained by assuming nonorthogonality of the Cu(II) z^2 and O_2^{2-} π^*_v orbitals due to distortion of each copper center away from an ideal trigonal bipyramidal geometry. This relates to our observations that the intensity of band I, the $\pi^*_v(O_2^{2-}) \rightarrow dz^2$(Co) transition, is strongly

(28) (a) Hester, R. E.; Nour, E. M. *J. Raman Spectrosc.* **1981**, *11*, 49. (b) Suzuki, M.; Ishiguro, T.; Nakamoto, K. *Inorg. Chem.* **1981**, *20*, 1993. (c) Nakamoto, K.; Suzuki, M.; Ishiguro, T.; Kozuka, M.; Nishida, Y.; Kida, S. *Inorg. Chem.* **1980**, *19*, 2822.

(29) Maecke, H. R.; Williams, A. F. In *Photoinduced Electron Transfer*; Fox, M. A., Chanon, M., Eds.; Elsevier: Amsterdam, 1988; Part D, p 28.

dependent on low-symmetry distortions. The second difference, i.e. the low-energy splitting between the π^*_v and π^*_σ transitions, indicates that excited-state interactions which should be different for the cobalt and the copper dimer, are important. The cobalt peroxo dimer is a closed-shell system; hence, triplet excited states should always be lower in energy than the corresponding singlets. In contrast, the copper dimer has two unpaired electrons, one on each copper center, and interactions in CT excited states can be strongly antiferromagnetic. It is interesting to note that, in agreement with this interpretation, SW-Xα calculations[30] predict a splitting between the π^*_v and π^*_σ transitions of 8500–23 000 cm^{-1} for a trans μ-1,2-peroxo copper dimer, which is much closer to the value observed for the cobalt dimer than for the copper dimer. Since the calculated value averages out excited-state exchange splittings, the difference between the theoretical and experimental values must be due to excited-state exchange interactions. In fact, large antiferromagnetic interactions have been observed in CT bands of dimers.[4c] We are now developing a general theoretical approach to describe and calculate charge-transfer excited-state dimer splittings.[31]

Acknowledgment. We thank R. Musselman and F. Fronczek for crystal structures of two systems and B. Hedman for assistance with the four-cycle diffractometer. F.T. acknowledges the Deutsche Forschungsgemeinschaft (DFG) for a postdoctoral fellowship, and E.I.S. thanks the NIH (Grant DK-31450) for support of this research.

Registry No. $[NH_3]SCN$, 18496-85-0; $[NH_3]NO_3SCN$, 138877-17-5; $[NH_3\text{-tren}]SCN$, 38967-82-7; $[NH_3\text{-tren}]SO_4$, 138856-07-2; [en-dien]-ClO_4, 40685-52-7.

(30) Ross, P. K.; Solomon, E. I. *J. Am. Chem. Soc.* **1991**, *113*, 3246.

(31) Tuczek, F.; Solomon, E. I. To be published.

Contribution from the Department of Chemistry, Kansas State University, Manhattan, Kansas 66506

(*o*-Phenylenediimido)- and (*p*-Phenylenediimido)ditungsten Complexes

Mong Liang and Eric A. Maatta*

Received September 12, 1991

The preparations of a series of dinuclear complexes of W(VI), W(V), and W(IV), bridged by either *o*- or *p*-phenylenediimido ligands, are described. The insoluble (and presumably polymeric) d^0–d^0 systems, *o*- and *p*-$[Cl_4W{\equiv}NC_6H_4N{\equiv}WCl_4]$, are obtained in high yield from the reactions of either *o*- or *p*-$Me_3SiNHC_6H_4NHSiMe_3$ with 2 equiv of WCl_6 in CH_2Cl_2 solution at room temperature. Upon treatment with tetrahydrofuran, these systems produce the soluble 16-electron complexes *o*- and *p*-$[(THF)Cl_4W{\equiv}NC_6H_4N{\equiv}WCl_4(THF)]$. It is proposed that the THF ligands occupy sites trans to the organoimido ligands in these systems. The THF ligands in the para-disubstituted complex are readily displaced by chloride ions upon treatment with [PPN]Cl to afford the decachloro dianion $[PPN]_2[Cl_5W{\equiv}NC_6H_4N{\equiv}WCl_5]$. The ortho- and para-disubstituted THF derivatives each undergo facile reduction in solution in the presence of tertiary phosphines L to produce the W(V)–W(V) (d^1–d^1) systems *o*- and *p*-$[L_2Cl_3W{\equiv}NC_6H_4N{\equiv}WCl_3L_2]$. ESR spectra are consistent with the adoption of the *mer*-trichloro, *trans*-bis(phosphine) geometry for these complexes. Preliminary studies of the magnetic properties of these d^1–d^1 systems throughout the temperature range 5–300 K have revealed antiferromagnetic behavior in *p*-$[L_2Cl_3W{\equiv}NC_6H_4N{\equiv}WCl_3L_2]$ (L = Et_2PhP) and in *o*-$[L_2Cl_3W{\equiv}NC_6H_4N{\equiv}WCl_3L_2]$ (L = Me_3P). When these W(V)–W(V) systems are treated with sodium amalgam in the presence of additional phosphine, diamagnetic W(IV)–W(IV) (d^2–d^2) systems are obtained in high yield. In the case of para-disubstituted system, the product has the stoichiometry $[L_3Cl_2W{\equiv}NC_6H_4N{\equiv}WCl_2L_3]$ (L = Et_2PhP), and NMR studies suggest the adoption of the *cis*-dichloro, *mer*-tris(phosphine) geometry. In the case of the ortho-disubstituted system, the stoichiometry of the product obtained appears to depend on the steric bulk of the phosphine ligand employed. Use of the compact Me_3P species allows coordination of three phosphines per W atom, and the product obtained is of the form $[L_3Cl_2W{\equiv}NC_6H_4N{=}W{=}Cl_2L_3]$; a *cis*-dichloro, *mer*-tris(phosphine) geometry is again indicated by NMR studies. In the case of the bulkier Et_2PhP ligand, the product incorporates only two phosphines per W atom and is of the form $[L_2Cl_2W{\equiv}NC_6H_4N{\equiv}WCl_2L_2]$; the observed equivalence of the phosphine ligands in this species can be accommodated by a structure derived from either a square-based pyramid or a trigonal bipyramid.

Introduction

In previous papers in this series, we have described the construction of a series of dinuclear systems of molybdenum[1] and rhenium[2] bridged by *p*-phenylenediimido ligands, for which *p*-phenylenediazide, $N_3C_6H_4N_3$, and *p*-phenylenebis(triphenylphosphineimine), $Ph_3P{=}NC_6H_4N{=}PPh_3$, respectively served as the sources of the phenylenediimido unit. Subsequently, Andersen[3] reported synthetic and magnetic studies on a pair of bimetallic uranium(V) systems containing *p*- and *m*-phenylenediimido bridges; the corresponding phenylenediazide reagents served as the sources of the bridging groups in this study. We have found that trimethylsilyl derivatives of arylenediamines can also serve to introduce arylenediimido ligands into a variety of transition metal frameworks, and we now report our studies on a series of dinuclear systems of W(VI), W(V), and W(IV) containing either *o*- or *p*-phenylenediimido bridges. The resulting frameworks are depicted below.

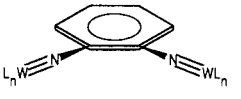

Results

Dinuclear Tungsten(VI) Systems. The reactions of either the 1,2- or the 1,4-isomer of *N,N'*-bis(trimethylsilyl)phenylenediamine with 2 equiv of WCl_6 proceed readily in CH_2Cl_2 solution at room temperature to provide the dinuclear W(VI) complexes *o*- and *p*-$[Cl_4W{\equiv}NC_6H_4N{\equiv}WCl_4]$, *o*-**1** and *p*-**1**, as shown in eq 1.[4] The

o- or *p*-$Me_3SiNHC_6H_4NHSiMe_3 + 2WCl_6 \rightarrow$
o- or *p*-$[Cl_4W{\equiv}NC_6H_4N{\equiv}WCl_4]$ (1)
o-**1**: ortho isomer
p-**1**: para isomer

products are obtained as greenish-brown powders in high yields (*o*-**1**, 79%; *p*-**1**, 90%), and both are virtually insoluble in nonco-

(1) Maatta, E. A.; Devore, D. D. *Angew. Chem., Int. Ed. Engl.* **1988**, *27*, 569.
(2) Maatta, E. A.; Kim, C. *Inorg. Chem.* **1989**, *28*, 623.
(3) Rosen, R. K.; Andersen, R. A.; Edelstein, N. M. *J. Am. Chem. Soc.* **1990**, *112*, 4588.

(4) The corresponding reaction of *N,N'*-bis(trimethylsilyl)-1,3-phenylenediamine with WCl_6 likewise affords the analogous meta-disubstituted system *m*-$[Cl_4W{\equiv}NC_6H_4N{\equiv}WCl_4]$, but we have not yet developed the chemistry of this complex: Maatta, E. A.; Jha, S. K. Unpublished results.

0020-1669/92/1331-0953$03.00/0